Available online at www.sciencedirect.com
ScienceDirect
Journal of Power Sources 159 (2006) 641–645
JOURNAL OF POWER SOURCES
www.elsevier.com/locate/jpowsour

Short communication

# Oxidation kinetics of Haynes 230 alloy in air at temperatures between 650 and 850 °C

Li Jian [a,*], Pu Jian [a], Hua Bing [a], Guangyuan Xie [b]

[a] School of Materials Science and Engineering, State Key Laboratory of Plastic Forming Simulation and Die and Mould Technology, Huazhong University of Science and Technology, Wuhan, Hubei 430074, PR China
[b] School of Materials Science and Metallurgical Engineering, Wuhan University of Science and Technology, Wuhan, Hubei 430080, PR China

Received 28 September 2005; accepted 30 September 2005
Available online 10 January 2006

**Abstract**

Haynes 230 alloy was oxidized in air at temperatures between 650 and 850 °C. Thermogravimetry was used to measure the kinetics of oxidation. The formed oxides were identified by the thin film (small angle) X-ray diffraction technique. $Cr_2O_3$ and $MnCr_2O_4$ were found in the oxide scale. Multi-stage oxidation kinetics was observed, and each stage follows Wagner's parabolic law. The first slow oxidation stage corresponded to the growth of an $Cr_2O_3$ layer, controlled by Cr ions diffusion through the dense $Cr_2O_3$ scale. The faster second stage was a result of rapid diffusion of Mn ions passing through the established $Cr_2O_3$ scale to form $MnCr_2O_4$ on top of the $Cr_2O_3$ layer. A duplex oxide scale is expected. The third stage, with a rate close to that of the first stage, only appeared for oxidation in the intermediate temperature range, i.e., 750–800 °C, which can be explained by the interruption of the Mn flux that forms $MnCr_2O_4$.


*Keywords:* Haynes 230; Kinetics; Oxidation; Multi-stage; Parabolic law

## 1. Introduction

With the development of the reduced temperature solid oxide fuel cells (SOFCs), metallic materials have drawn extensive attention as the interconnect materials [1–4]. The interconnect in a planar SOFC stack is a critical component that separates the fuel and oxidant gases and provides electric connection between the adjacent cells. In some stack designs, the interconnect is also a structural element to sustain the mechanical stability of the stack and to offer a mechanical connection surface for gas path sealing.

While most of the researchers have been focusing on the Fe–Cr ferritic stainless steels, Haynes 230 alloy, a Ni-based alloy, has entertained some investigators' interests as a potential interconnect material candidate [5–8]. Haynes 230 is an austenitic alloy with a coefficient of thermal expansion (CTE) of $15.2 \times 10^{-6}$ [9] between 25 and 800 °C, slightly higher than that of the ferritic stainless steels ($\sim 12 \times 10^{-6}$) and SOFC cell components ($10–13 \times 10^{-6}$ [10]), which has made it less popular than the Fe–Cr alloys for the interconnection applications. However, in most of planar SOFC stack designs, the interconnect is not strongly bonded to the cells, so that the magnitude of the CTE difference is believed to be acceptable without causing significant damage to the interconnect-cell contact. England et al. [5,6] studied the oxidation kinetics of thin foil Haynes 230 in humidified hydrogen and air at temperatures between 700 and 1100 °C for up to 10,000 h. It was found that $Cr_2O_3$ and $MnCr_2O_4$ were formed in both atmospheres following the parabolic law, and the area-specific resistance (ASR) on the anode side was higher than that of the cathode side. At 800 °C in air after 10,000 h, the ASR was $\sim 1.1\ \Omega\,cm^2$ which was considered unsatisfactory for the interconnect application. Li et al. [7,8] investigated the oxidation behavior of Haynes 230 sheet in simulated SOFC environments at 750 °C for 1000 h. Ni-rich nodules were identified on top of the oxide scale in the anodic atmosphere other than $Cr_2O_3$ and $MnCr_2O_4$ due to the low oxygen partial pressure which is not sufficient to oxidize the Ni element in the alloy; and the estimated ASR suggested that Haynes 230 may be suitable as an alternative interconnect material.

* Corresponding author. Tel.: +86 27 87557694; fax: +86 27 87544307.
*E-mail address:* plumarrow@126.com (L. Jian).

0378-7753/$ – see front matter © 2005 Elsevier B.V. All rights reserved.
doi:10.1016/j.jpowsour.2005.09.065

The objective of the present study was to examine the oxidation kinetics and associated oxide formation in air at temperatures between 650 and 850 °C where the reduced temperature SOFCs operate. The oxidation kinetics was obtained by weighing oxidized samples, and the formed surface oxides with time were tracked and identified by the small-angle X-ray diffraction technique.

## 2. Experimental

Haynes 230 alloy was provided by Haynes International, its nominal chemical composition is listed in Table 1. Coupons of 25 mm × 25 mm × 1 mm were prepared by using an electron discharge machine. The sample surfaces were polished with SiC abrasive papers up to 1200-grit, and washed in an ultrasonic cleaner in distilled water and acetone.

The weight of the cleaned and dried samples was recorded prior to the oxidation test. Thermogravimetry was employed to study the oxidation kinetics. The samples were heated in air with a box furnace at 650, 750 and 850 °C, respectively, and held for up to 500 h. The weight gain with oxidation time was obtained by weighing different samples every 100 h using a Sartorius BS 124S electronic balance (accuracy of $10^{-4}$ g).

Since the thickness of the oxide scale formed on the alloy surface is in the order of microns, the thin film (small angle) X-ray diffraction technique was employed to identify the surface oxides. The angle between the incident beam and the oxidized surface was fixed at in the range between 0.5 and 1.2°, while the detector rotated continuously along the goniometer to receive the diffraction signals. A PANalytical X'Pert PRO X-ray diffractometer was used for this purpose under the conditions of 40 mA and 40 kV; the scanning speed was 10° $min^{-1}$, and the 2$\theta$ angle ranged from 20 to 80°.

## 3. Results and discussions

Figs. 1–3 illustrate the dependence of the weight gain of the samples on the oxidation time in stagnant air (atm.) at 650, 750 and 850 °C, respectively. The (weight gain/area)$^2$ is plotted as a function of the time. At all three oxidation temperatures, at least two linear relationships were observed within 500 h of oxidation, which suggests a multi-stage oxidation and each stage obeys parabolic kinetics. The oxidation stage transfer occurred after 200 h of oxidation and it was delayed with decrease of the oxidation temperature. The slope of each straight line represents the experimentally obtained parabolic rate constant $k_W$ in terms of the weight change:

$$\Delta W^2 = k_W t \quad (1)$$

and is listed in Table 2, where $\Delta W$ is the specific area weight gain (mg $cm^{-2}$) of the sample and $t$ is the oxidation time. For the oxidation at 750 °C, it is also noted that the (weight gain/area)$^2$ ~oxidation time curve tends to bend away from the second stage after 400 h of oxidation, the oxidation rate is slowed down to the magnitude of the first stage. A similar phenomenon was

Table 1
Chemical composition of Haynes 230 alloy

| Element | wt.% |
|---|---|
| Ni | 57 |
| Cr | 22 |
| W | 14 |
| Mo | 2.0 |
| Mn | 0.5 |
| Si | 0.4 |
| Al | 0.3 |
| C | 0.1 |
| La | 0.02 |
| Co | 5.0 |
| Fe | 3.0 |
| B | 0.01 |

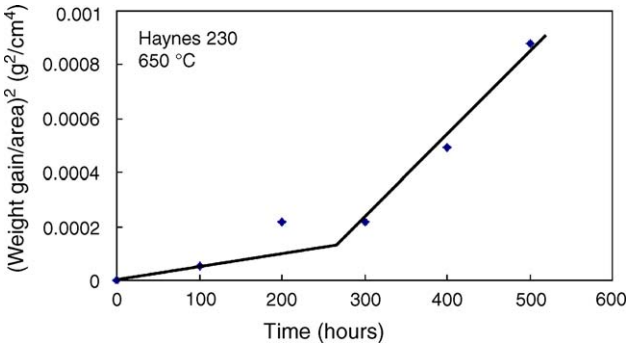


Fig. 1. Weight gain as a function of oxidation time for Haynes 230 alloy oxidized at 650 °C in air.

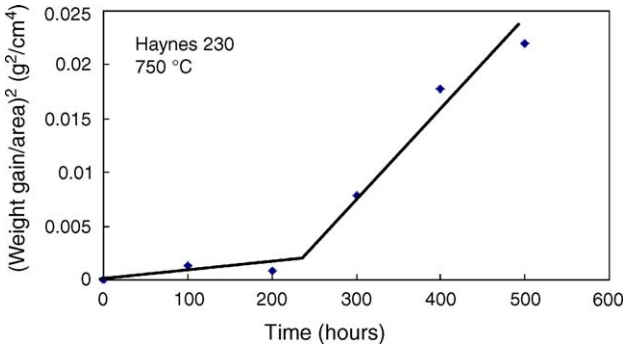


Fig. 2. Weight gain as a function of oxidation time for Haynes 230 alloy oxidized at 750 °C in air.

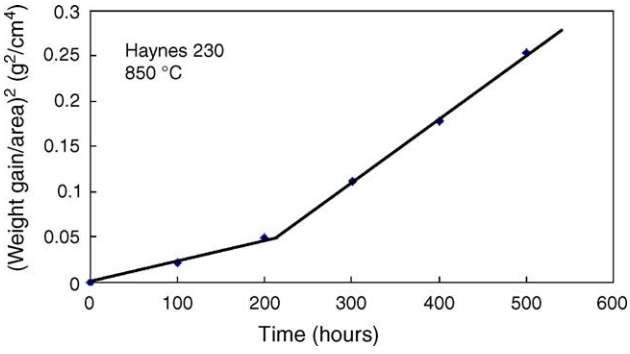


Fig. 3. Weight gain as a function of oxidation time for Haynes 230 alloy oxidized at 850 °C in air.

Table 2
Experimentally obtained parabolic rate constant $k_w$ ($g^2\,cm^{-4}\,s^{-1}$) for each oxidation stage at various temperatures, and the determined activation energy $Q$ (kJ/mol)

| Parabolic rate constants | 650 °C | 750 °C | 850 °C | $Q$ |
|---|---|---|---|---|
| $k_w^{(1)}$ | $3.05 \times 10^{-16}$ | $1.22 \times 10^{-15}$ | $6.68 \times 10^{-14}$ | 252 |
| $k_w^{(2)}$ | $9.14 \times 10^{-16}$ | $2.03 \times 10^{-14}$ | $1.89 \times 10^{-13}$ | 216 |

observed in the previous study [11] where Haynes 230 alloy sheet (1 mm thick) was oxidized in air at 800 °C for up to 1000 h, as shown in Fig. 4, three straight lines were obtained and the slope of the first and the third lines has almost the same value. All in all, these results have confirmed that multi-stage oxidation occurs with prolonged oxidation at high temperature for Haynes 230 alloy, and each stage is a diffusion controlled process. The rate constant can be expressed by the Arrhenius equation

$$k_W = k_{W_0} \exp\left(-\frac{Q}{RT}\right) \quad (2)$$

where $k_{W_0}$ is the pre-exponential factor, $Q$ is the activation energy, $R$ is the gas constant and $T$ is the absolute temperature, and further more,

$$\ln k_W = -\frac{Q}{R}\left(\frac{1}{T}\right) + \ln k_{W_0} \quad (3)$$

Fig. 5 illustrates the experimental relationship between ln $k_W$ and $1/T$ for oxidations at various temperatures in each stage, a linear relation is demonstrated and Eq. (3) is satisfied. The derived activation energy $Q$ for each stage are also listed in Table 2.

Figs. 6–8 are the thin film (small angle) X-ray diffraction results from the surfaces of Haynes 230 samples oxidized at 650, 750 and 850 °C for different times, respectively. All the oxide scales contain $Cr_2O_3$ and spinel-type $MnCr_2O_4$ phases. However, the relative amount of each oxide within the penetration depth of the small angle X-ray changes with the oxidation time, the intensity of diffraction peaks from $MnCr_2O_4$ gradually increases while those from $Cr_2O_3$ gradually decrease, suggesting the growth of $MnCr_2O_4$ on top of $Cr_2O_3$ and a duplex oxide scale. With the growth of $MnCr_2O_4$ intensified, the oxidation kinetics switches from the first stage to the second, as seen in

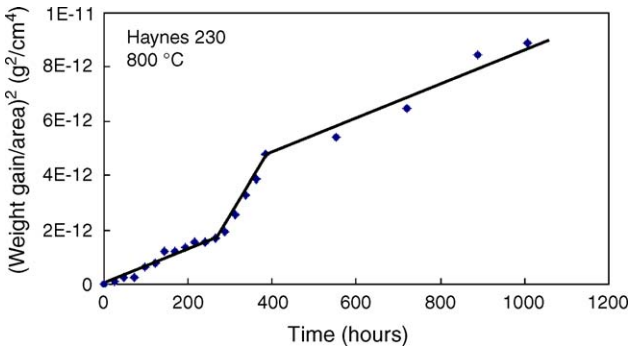


Fig. 4. Weight gain as a function of oxidation time for Haynes 230 alloy oxidized at 800 °C in air.

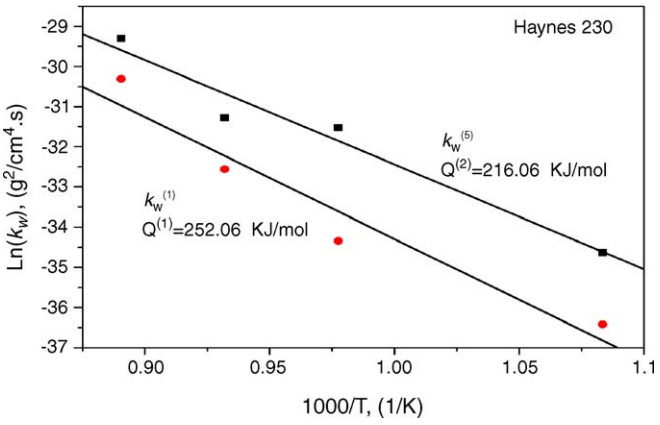


Fig. 5. Dependence of parabolic rate constant on temperature for Haynes 230 alloy oxidized at temperatures between 650 and 850 °C. The rate constant for each stage is plotted separately.

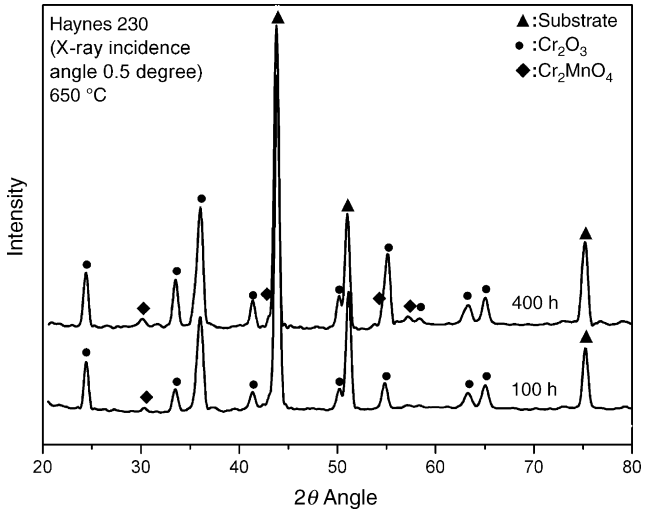


Fig. 6. Small angle X-ray diffraction patterns for Haynes 230 alloy oxidized in air at 650 °C for different time.

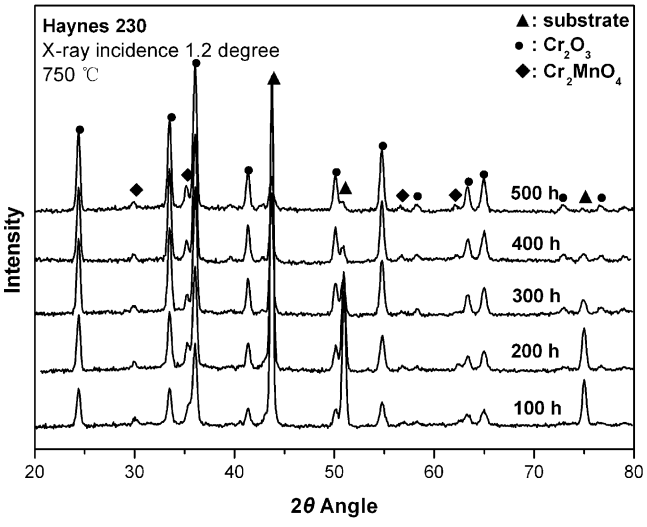


Fig. 7. Small angle X-ray diffraction patterns for Haynes 230 alloy oxidized in air at 750 °C for up to 500 h.

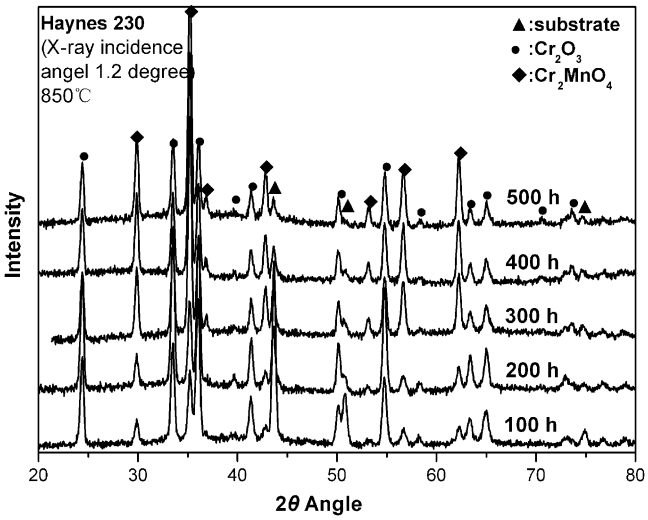


Fig. 8. Small angle X-ray diffraction patterns for Haynes 230 alloy oxidized in air at 850 °C for up to 500 h.

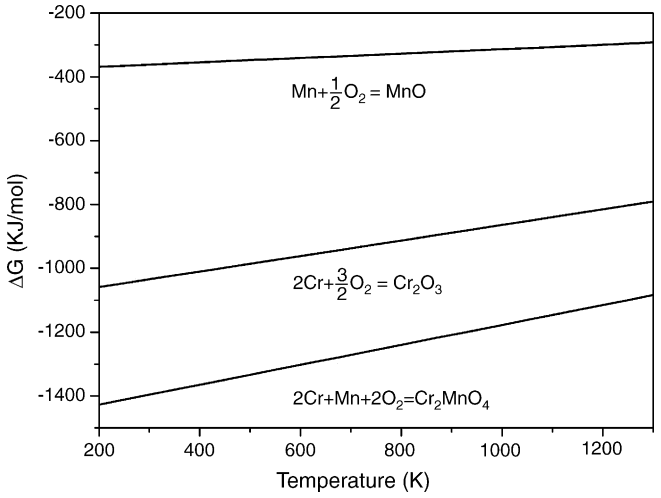


Fig. 9. Dependence of standard Gibbs free energy of formation on temperature for $Cr_2O_3$, MnO and $MnCr_2O_4$ phases.

Figs. 1–3. This phenomenon can be seen in the case of oxidation at 750 and 850 °C. For oxidation at 650 °C, the oxide scale is extremely thin; the signal from the substrate is significantly strong so that the small amount of $MnCr_2O_4$ can be barely detected even after 400 h of oxidation.

Multi-stage oxidation has not been previously reported in Haynes 230 alloy, however, it has been observed in other alloys [12–15]. Marasco and Young [12] described the oxidation of Fe–Cr–Mn alloys at 900 °C in air, and up to three stages of oxidation were found. They attributed the multi-stage oxidation to the formation of $M_3O_4$-type (M: Fe, Cr or Mn) and $M_2O_3$-type oxides. The formation of $M_3O_4$ oxide is preceded by the growth of $M_2O_3$ oxide, and the growth rate of $M_3O_4$ is considered an order of magnitude greater than that of $M_2O_3$. Cox [13] proposed a similar mechanism for the oxidation of Fe–Cr alloys to explain the transition from the initial slow oxidation to the faster rate characteristic of the formation of thicker duplex oxide scales. It was observed that the number of $M_3O_4$ spinel nuclei remains essentially constant after the initial period but they increase in size relatively quickly to cover the entire surface. This observation is consistent with what Caplan [14] concluded. In Fe–Cr–Mn alloys, the Mn rapidly diffuses from the alloy to the surface to form Mn-rich oxide, causing severe local Mn depletion. The underlying alloy adjacent to the Mn-rich oxide scale has a transient composition approximating to the Fe–Cr alloy unit: the Mn flux is re-established, resulting in formation of $Cr_2O_3$. Fig. 9 [15] shows the dependence of standard Gibbs free energy of formation of $Cr_2O_3$, MnO and $MnCr_2O_4$ phases on temperature. $MnCr_2O_4$ is thermodynamically a more favorable phase than $Cr_2O_3$ and MnO, a few tenths of a percent of Mn added to a binary Fe–Cr alloy, which is not avoidable in most of the Fe–Cr alloys, lead to the formation of $MnCr_2O_4$ phase.

In Haynes 230 alloy, the Mn content is around 0.5 wt.% which is much lower than that of the Cr 22 wt.% At the very beginning of the oxidation, the Mn and Cr on the surface forms $MnCr_2O_4$, and a Mn depletion zone as well, while the remaining Cr forms a dense layer of $Cr_2O_3$ in the first stage, Cr ions diffusion passing this dense $Cr_2O_3$ layer controls the oxidation kinetics, with insignificant growth of $MnCr_2O_4$. The experimentally obtained activation energy for the first stage is around 252 kJ $mol^{-1}$, which is in good agreement with the reported activation energies [5] for Cr diffusion in $Cr_2O_3$ oxide. Owing to the sluggish diffusion of Cr ions in $Cr_2O_3$ scale [16], the oxidation rate is relatively slow. The second stage oxidation corresponds to the growth of $MnCr_2O_4$ after the re-establishment of the Mn flux. The content of Mn in the present alloy is quite low; the re-establishment may take longer time than that in the higher Mn content alloys [12]. The time needed for the Mn flux re-establishment is also temperature dependant, and a longer time is required for lower oxidation temperature, as demonstrated in Figs. 1–3. $MnCr_2O_4$ forms at the gas-scale interface, and thickens as a result of Mn ion diffusion through $Cr_2O_3$. As is well known, Mn ions diffusion is orders of magnitude faster than Cr ions in $Cr_2O_3$ [16], resulting in a rapid oxidation rate in the second stage. In order to maintain the growth of $MnCr_2O_4$, the Mn diffusion flux must reflect with the growth rate; so a continuous supply of Mn is needed. Because of the limitation of Mn content in Haynes 230 alloy, after a period of fast growth of $MnCr_2O4$, the requirement for a continuous supply of the Mn flux may not be able to be satisfied. Such Mn depletion may interrupt the growth of $MnCr_2O_4$, and then the oxidation kinetics turns into a third stage, controlled by Cr diffusion to form $Cr_2O_3$ on top of $MnCr_2O_4$. This explains the second slope change in Fig. 4 to a value similar to that of the first stage. It is noticed that this second change of oxidation kinetics with time did not happen in the present study within 500 h of oxidation. The observation in the previous study [11] reported the second oxidation kinetic change occurred at around 400 h of oxidation. The difference may be caused by the Haynes 230 samples coming from different batches, the Mn content may have slightly varied.

According to Wagner's parabolic oxidation theory, the oxidation rate of alloys is governed by the diffusion of cations passing a dense oxide scale and the rate constant is a function of concentration and self-diffusion coefficient of the migrating species. For the present situation in which both $Cr_2O_3$ and $MnCr_2O_4$ form

simultaneously with rates of $k_{(Cr_2O_3)}$ and $k_{(MnCr_2O_4)}$, respectively, in terms of specific area weight gain $\Delta W_{(Cr_2O_3)}$ and $\Delta W_{(MnCr_2O_4)}$, then

$$\Delta W^2_{(Cr_2O_3)} = k_{(Cr_2O_3)}t \quad (4)$$

$$\Delta W^2_{(MnCr_2O_4)} = k_{(MnCr_2O_4)}t \quad (5)$$

For the overall weight gain $\Delta W$, it has

$$\Delta W^2 = k_W t \quad (1)$$

and

$$\Delta W = \Delta W_{(Cr_2O_3)} + \Delta W_{(MnCr_2O_4)} \quad (6)$$

Substituting (1), (4) and (5) into (6), the relation between $k_{(Cr_2O_3)}$, $k_{(MnCr_2O_4)}$ and $k_W$ is given by

$$k_W^{1/2} = k_{(Cr_2O_3)}^{1/2} + k_{(MnCr_2O_4)}^{1/2} \quad (7)$$

In the first stage of oxidation, $k_{(Cr_2O_3)}$ controls the overall kinetics due to the initial Mn depletion. In the second stage, both $k_{(Cr_2O_3)}$ and $k_{(MnCr_2O_4)}$ contribute to $k_W$, resulting in faster oxidation kinetics with smaller activation energy. And in the third stage, the Cr diffusion resumes the control of the oxidation kinetics due to the interruption of the Mn flux that maintains the $MnCr_2O_4$ formation.

## 4. Conclusions

Oxidized at temperatures between 650 and 850 °C, Haynes 230 alloy demonstrates multi-stage oxidation kinetics, and each stage follows a parabolic rate law. Only two types of oxide, $Cr_2O_3$ and $MnCr_2O_4$, are identified for oxidation at all temperatures during the period of testing time (500 h). The first slow oxidation stage corresponded to the growth of a $Cr_2O_3$ layer, controlled by Cr ion diffusion through the dense $Cr_2O_3$ scale. The oxidation rate is faster in the second stage due to the fast diffusion of Mn ions passing through the established $Cr_2O_3$ scale to form $MnCr_2O_4$ on top of the $Cr_2O_3$ layer. A duplex oxide scale is expected. The third stage only appears after oxidation for a certain period of time, when the continuation of the Mn flux to form $MnCr_2O_4$ is interrupted due to the limited Mn supply and Cr diffusion resumes the control of the oxidation kinetics in this stage.

## Acknowledgement

This research has been financially supported by the National Science Foundation of China under the project contract 50471063 and the "863" high-tech project under the contract 204AA32G070.

## References

[1] J.M. Ralph, A.C. Schoeler, M. Krumpelt, Materials for lower temperature solid oxide fuel cells, J. Mater. Sci. 36 (2001) 1161–1172.
[2] W.Z. Zhu, S.C. Deevi, Development of interconnect materials for solid oxide fuel cells, Mater. Sci. Eng. A348 (2003) 227–243.
[3] W.J. Quadakkers, J. Piron-Abellan, V. Shemet, L. Singheiser, Metallic interconnectors for solid oxide fuel cells—a review, Mater. High Temperatures 20 (2) (2003) 115–127.
[4] W.Z. Zhu, S.C. Deevi, Opportunity of metallic interconnects for solid oxide fuel cells: a status on contact resistance, Mater. Res. Bull. 38 (2003) 957–972.
[5] D. England, A. Virkar, Oxidation Kinetics of some nickel-based superalloy foils and electronic resistance of the oxide scale formed in air, J. Electrochem. Soc. 146 (1999) 3196–3202.
[6] D. England, A. Virkar, Oxidation Kinetics of some nickel-based superalloy foils in humidified hydrogen and electronic resistance of the oxide scale formed, J. Electrochem. Soc. 148 (2001) A330–A338.
[7] L. Jian, P. Jian, X. Jianzhong, Q. Xiaoliang, Oxidation of Haynes 230 alloy in reduced temperature solid oxide fuel cell environments, J. Power Sources 139 (2005) 182–187.
[8] L. Jian, P. Jian, G. Xie, W. Shunxu, Heat resistant alloys as interconnect materials of reduced temperature SOFCs, J. Power Sources, in press.
[9] Haynes 230 Alloy Product Brochure, Haynes International.
[10] Fuel Cell Handbook, The US Department of Energy, 2004.
[11] Li Jian, unpublished work, 2003.
[12] A.L. Marasco, D.J. Young, The oxidation of iron–chromium–manganese alloys at 900 °C, Oxidation Metals 36 (1–2) (1991) 157–174.
[13] M.G.C. Cox, Kinetics of initial oxide growth on Fe–Cr alloys and the role of vacancies in film breakdown, Philosophical Magazine 31 (2) (1975) 331–338.
[14] D. Caplan, P.E. Beaubien, M. Cohen, Trans. AIME 233 (1965) 766.
[15] P. Jian, L. Jian, H. Bing, G. Xie, Oxidation kinetics and phase evolution of a Fe–16Cr alloy in simulated SOFC cathode atmosphere, J. Power Sources, in press.
[16] R.E. Lobnig, H.P. Schmidt, K. Hennesen, H.J. Grabke, Diffusion of cations in chromia layers grown on iron-base alloys, Oxidation Metals 37 (1/2) (1992) 81–93.